

Relativistic (e, 2e) study with twisted electron beam on heavy atomic targets

Aditi Mandal,¹ Nikita Dhankhar,¹ Didier Sébilleau,² and Rakesh Choubisa^{1,*}

¹*Department of Physics, Birla Institute of Technology and Science-Pilani,
Pilani Campus, Pilani, Rajasthan, 333031, India*

²*Univ Rennes, CNRS, IPR (Institut de Physique de Rennes) - UMR 6251, F-35000 Rennes, France*

In this communication, we report our calculations of Triple Differential Cross-Section (TDCS) for relativistic (e,2e) with twisted electron beam on heavy atomic targets, namely Cu, Au and Ag, in coplanar asymmetric geometry mode. The formalism has been developed in the first Born approximation using the Dirac plane wave as well as the twisted electron wave for the incident electron to study the effect of various parameters of the twisted electron on the relativistic (e,2e) process. We use Dirac plane wave, semi relativistic Coulomb wave and Darwin wave function for the scattered, ejected and K-shell electron respectively. We compare the angular profile of the TDCS for different values of Orbital Angular Momentum (OAM) (m) of the twisted electron with that of the plane wave. We segregate the TDCS for charge-charge interaction and current-current interaction with their interference term and study the effect of various parameters of the twisted electron beam on them, namely opening angle (θ_p), OAM number (m) and impact parameter (b). The spin asymmetry in TDCS caused by polarized incident electron beam is also studied to elucidate the effects of twisted electron beam on relativistic (e,2e) process.

PACS numbers:

I. INTRODUCTION

The coincidence (e, 2e) study on atoms and molecules have been explored for last five decades for the impact energy ranging from low energy to relativistic energy regime for numerous targets. (e, 2e) process has a long history in atomic and molecular physics. Observation of momentum distribution of electrons in individual atomic and molecular shells was initially suggested by McCarthy et. al. around 1960 [1]. Originally derived for the (p, 2p) spectroscopy in nuclear physics [2], where p represents a proton, it was proposed in 1966 by Smirnov and co-workers [3] for the investigation of atomic wave functions [4], upon the replacement of the protons by electrons. Since then, it has enjoyed a widespread applications such as electron momentum spectroscopy [5]. In many branches of physics, such as astrophysics and plasma physics, there has been considerable interest for the study of ionization processes by charged particle. The electron-impact single ionization, called the (e, 2e) process, has thus become a powerful tool for investigating the dynamics of the ionization process [6]. The coincidence cross sections, here defined as Triple Differential Cross Sections (TDCS), depend on the momenta of two outgoing electrons (here scattered and the ejected electron). Since the first (e, 2e) measurements reported independently in the late 1960s by Ehrhardt et al. [7] and Amaldi et al. [8], experimental and theoretical activities in the non-relativistic energy scale have been intense (e.g. see [9–11]). The (e,2e) study is still being explored, particularly on molecular targets. A short time ago, BBK, BBKDW and BBKSR theoretical mod-

els have been used to study argon atom and some specific molecules like H_2O , CH_4 and NH_3 [12]. In all the above mentioned works, the electron impact energy lies in a energy range typically between 10 eV and 10 keV, wherein the spin aspects do not play major role except in anti symmetrization of the wave-function of involving electrons. Work in the relativistic energy regime started in 1982 by Schule and Nakel [13] who reported absolute (e, 2e) experiments on the K shell of Silver atom at an incident energy of 500 keV. The aim of such types of kinematically complete relativistic (e, 2e) experiments was probe the fundamental ionization mechanism at relativistic energies and strong fields of the K shell of heavier atoms. Later on, experiments have been performed with transversely polarized electron beams [14] representing an ideal complete quantum mechanical scattering experiment where in, apart from the momenta, the spin of impinging beam is also resolved. These (e,2e) experiments have entailed the development of new theoretical and computational methods [15].

Recently, there has been new interesting breakthroughs, arising from the ability to bestow orbital angular momentum (OAM) to the wave function of electrons and it is termed as “*twisted* electrons” [16]. Hence with this, now we would be able to probe multiple sources of perturbation. Initially the concept of twisted Photons came in picture and accordingly as cited in [17] “researchers have begun to appreciate its implications for our understanding of the many ways in which light and matter can interact, or its practical potential for quantum information” applications. In similar lines, *twisted* electrons are now being explored. *Twisted* electrons are not plane waves, but superposition of plane waves with a defined projection of the orbital angular momentum onto the propagation axis. This projection, which nowadays can be very high [18], determines the magnitude

*Electronic address: rchoubisa@pilani.bits-pilani.ac.in

of the OAM induced magnetic moment. Due to large magnetic dipole moment, twisted electrons can be used as a valuable tool for studying the magnetic properties of materials at nanoscale [19–21].

In recent past, Serbo et al [22] used relativistic first Born approximation to study the Mott scattering of highly energetic twisted electrons by atoms and macroscopic targets. A generalised Born approximation has been developed in order to investigate scattering of the vortex electron by atomic targets [23]. As concluded in [24–27], the cross-section of twisted wave is comparable to that for the standard plane-wave. And this idea can be employed for any type of electron-atom interaction which may lead to ionization process, like (e,2e) and (e,3e) processes. In the coincidence (e,2e) process, we detect all the participating particles in the continuum state with their momenta fully resolved. Naturally considering the twisted electron in place of standard plane-wave regime will extract more information about the (e,2e) processes as available presently. Till now, almost all of the (e,2e) activities have been confined to electron beam which carries linear momentum in its impinging direction except the recent study by Harris et al [28] in which TDCS for non-relativistic (e,2e) processes using twisted electron beam has been explored. To the best of our knowledge, the relativistic (e, 2e) processes on atomic target with twisted electron has not been explored in the literature, even the theoretical estimation is not explored. As mentioned earlier, the twisted electron carries orbital angular momentum in addition to linear momentum, it will be an interesting task to probe the effects of OAM of the twisted electrons on the (e, 2e) processes on atoms especially at relativistic energy range. Further, one can also probe the effect of twisted electron on the spin asymmetry in TDCS. In addition to this, it would be interesting task to investigate the effect of impact parameters of the twisted electron on the (e,2e) processes. The present communication is intended to cover these aspects in theoretical manner. We hope that the present results may stimulate theoretical and experimental studies on relativistic (e,2e) processes with twisted electron impact on atoms. Here we present our calculation of TDCS and spin asymmetry for K-shell ionization of Cu,Ag and Au targets for twisted electron case.

The paper is organised as follows, followed by the Introduction, we describe the essential theory for the computations of TDCS and spin asymmetry in TDCS for the relativistic (e,2e) processes on atoms with plane and twisted electron beam in the "Theoretical Formalism" section. We discuss our theoretical results of TDCS and spin asymmetry in the "Results and Discussion" section. Finally we conclude our findings in the "Conclusion" section.

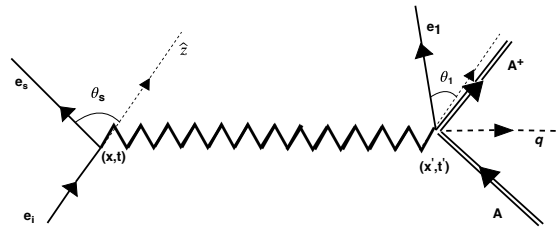


FIG. 1: Schematic diagram for (e,2e) process on atom (A) by an incident electron (e_i) in one photon-exchange approximation. The wavy line is for virtual photon, responsible for the electron-atom interaction and points along the direction of momentum transfer (θ_q , from the incident electron direction). The incident electron scatters at θ_s angle and the ejected electron ejects at θ_1 direction from the incident direction (z-axis) in the scattering plane defined in the xz-plane. The geometry here used is coplanar asymmetric ($E_s > E_1$).

II. THEORETICAL FORMALISM

The theoretical formalism has been developed with following assumptions:

(1) We assume that the electron-atom collision is of first order in which a virtual photon is emitted by the incident electron at (x,t) along the direction of momentum transfer which is absorbed by the atom at (x',t') (see Fig.1). The interaction leads to the ejection of the K-shell electron of atom and the incident electron is scattered by an angle θ_s .

(2) The ejected electron is ejected in the θ_1 direction from the direction of the incident electron. All the electrons are in same plane (scattering plane). For the incident electron beam, we use Dirac plane wave function for plane wave incidence and the Bessel wave function, which represents superposition of plane waves, for twisted electron incidence.

(3) We describe Dirac plane wave function, semi relativistic Coulomb wave function and Darwin wave function for the scattered, ejected and K-shell electron respectively. TDCS is computed here in the coplanar asymmetric geometry ($E_s > E_1$).

A. Plane wave ionization

In the (e,2e) process on atom, we compute the differential cross sections in various kinematic arrangements of the outgoing electrons involved in the ionization process. The ionization of an atomic target by an electron may be framed as [6]:

$$e_i^- + A \longrightarrow A^+ + e_s^- + e_1^- . \quad (1)$$

where i,s and 1 represent incident,scattered and ejected electron with A being the target. In the coincident (e,2e) experiment, the momenta of the scattered and ejected electrons in the continuum state are resolved and hence the coincidence cross-section (here TDCS) depends on

energy and directions of the electron. We can compute the relativistic TDCS corresponding to an (e,2e) process in the first Born approximation as:

$$\frac{d^3\sigma}{d\Omega_s d\Omega_1 dE_s} = (2\pi)^4 \frac{k_s k_1}{k_i} \frac{E_i E_s E_1}{c^6} \overline{\sum_{\varepsilon_i \varepsilon_b \varepsilon_s \varepsilon_1}} |\langle f | \widehat{S} | i \rangle|^2. \quad (2)$$

As explained in [28], in the context of (e,3e) process, here for the case of (e,2e), \widehat{S} is the S-matrix operator; $\varepsilon_i, \varepsilon_s, \varepsilon_b$ and ε_1 refer to the spin projection of the incoming, scattered, bound (K-shell) and ejected electrons in the continuum state respectively. E_i, E_s, E_1 and k_i, k_s, k_1 are the on-shell total energies and momenta of the unbound particles. The spin projections are taken with respect to the propagation direction of incident electron beam (also defined as z-axis).

Here, TDCS is calculated as an average over initial-state spins of the incident electron and bound electron and a sum over final-state spins of the scattered and ejected electrons. The main task here is to calculate the S-matrix element in the following form [29]:

$$\langle f | \widehat{S} | i \rangle = \frac{-1}{c} \int \mathbf{A}_\mu(r_1) \mathbf{J}^\mu(r_1) d^3 r_1, \quad (3)$$

where $\mathbf{A}_\mu(r_1)$ can be expressed as

$$\mathbf{A}^\mu(r_1) = \frac{4\pi}{(2\pi)^3} \frac{[u^\dagger(k_s, \varepsilon_s) \gamma^0 \gamma^\mu u(k_i, \varepsilon_i)]}{[q^2 - (\frac{\Delta E}{c})^2]} [e^{i\mathbf{q}\cdot\mathbf{r}_1}]. \quad (4)$$

Here $\mathbf{q} = \mathbf{k}_i - \mathbf{k}_s$ is the momentum transfer, $\Delta E = E_i - E_s$, γ^μ are Dirac matrices, $u(k_i, \varepsilon_i)$ and $u(k_s, \varepsilon_s)$ are Dirac spinors of following form:

$$u_{k,\lambda} = N \begin{pmatrix} n_z + 1 \\ n_x + in_y \\ \frac{ck}{E_k + c^2} (n_z + 1) \\ \frac{ck}{E_k + c^2} (n_x + in_y) \end{pmatrix}, \quad (5)$$

$$u_{k,-\lambda} = N \begin{pmatrix} -n_x + in_y \\ n_z + 1 \\ -\frac{ck}{E_k + c^2} (-n_x + in_y) \\ -\frac{ck}{E_k + c^2} (n_z + 1) \end{pmatrix}, \quad (6)$$

where (n_x, n_y, n_z) are components of unit vectors of electron's momentum along x,y and z direction. The quantum number $+\lambda$ and $-\lambda$ attached to the spinors are helicity which represent right-handed and left-handed polarization respectively of the electrons (projection of spin along beam direction). The atomic transition four-current density for the electron transition from the K shell to the continuum state ($J^\mu(r_1)$) is defined as:

$$J^\mu(r_1) = c \psi_f^\dagger(r_1) \gamma^0 \gamma^\mu \psi_i(r_1), \quad (7)$$

where ψ_f is the semi relativistic Coulomb wave function,

$$\psi_f(r_1) = \phi_{k_1}(Z, r_1) u(k_1, \varepsilon_1), \quad (8)$$

where $\phi_{k_1}(Z, r_1)$ is Coulomb wave-function defined as

$$\phi_{k_1}(Z_1, r_1) = \frac{1}{(2\pi)^{3/2}} e^{i\mathbf{k}_1 \cdot \mathbf{r}_1} \exp\left(\frac{\pi Z}{2k_1}\right) \Gamma\left(1 + i\frac{Z}{k_1}\right) {}_1F_1\left(\frac{-iZ}{k_1}, 1, -i(k_1 r_1 + \mathbf{k}_1 \cdot \mathbf{r}_1)\right), \quad (9)$$

where Z is atomic number.

While, $\psi_i(r_1)$ is Darwin wave function for K-shell electrons [30] with following form:

$$\psi_i(r_1) = Z'^3 [a_{s_b}(\varepsilon_b)] e^{-Z' r_1}. \quad (10)$$

Here, $Z' = Z - 0.3$ is the effective nuclear charge and a_{s_b} is Darwin matrix [30] of the following form (in atomic units) for both spin polarization:

$$a_{s_b}(\uparrow) = \begin{pmatrix} 1 \\ 0 \\ \frac{1}{2ic} \frac{\delta}{\delta z} \\ \frac{1}{2ic} \left(\frac{\delta}{\delta x} + i \frac{\delta}{\delta y} \right) \end{pmatrix}, \quad (11)$$

$$a_{s_b}(\downarrow) = \begin{pmatrix} 0 \\ 1 \\ \frac{1}{2ic} \left(\frac{\delta}{\delta x} - i \frac{\delta}{\delta y} \right) \\ \frac{1}{2ic} \frac{\delta}{\delta z} \end{pmatrix}. \quad (12)$$

The matrix element for charge-charge interaction can be described as:

$$\langle f | \widehat{S} | i \rangle_0 = -\frac{1}{c} \int A_0(r_1) J^0(r_1) d^3 r_1. \quad (13)$$

Similarly the matrix element for current-current interaction becomes

$$\langle f | \widehat{S} | i \rangle_J = -\frac{1}{c} \int A_\mu(r_1) J^\mu(r_1) d^3 r_1, \quad (14)$$

where, $\mu = x, y, z$. The total contribution $\langle f | \widehat{S} | i \rangle$ can be written as

$$\langle f | \widehat{S} | i \rangle = \langle f | \widehat{S} | i \rangle_0 - \langle f | \widehat{S} | i \rangle_J. \quad (15)$$

We can compute $(TDCS)_0, (TDCS)_J$ and $(TDCS)_T$ respectively from equation (13), (14) and (15) by squaring the corresponding the S-matrix element.

In the calculation of matrix element $\langle f | \widehat{S} | i \rangle$, we encounter the following types of spatial integrals [29]:

$$I_1 = \int \phi_k^*(r) e^{i\mathbf{q}\cdot\mathbf{r}} e^{-Z' r} d^3 r, \quad (16)$$

$$I_2 = \int \phi_k^*(r) e^{i\mathbf{q}\cdot\mathbf{r}} \frac{\delta}{\delta x} e^{-Z' r} d^3 r, \quad (17)$$

$$I_3 = \int \phi_k^*(r) e^{i\mathbf{q}\cdot\mathbf{r}} \frac{\delta}{\delta y} e^{-Z' r} d^3 r, \quad (18)$$

$$I_4 = \int \phi_k^*(r) e^{i\mathbf{q}\cdot\mathbf{r}} \frac{\delta}{\delta z} e^{-Z'r} d^3r, \quad (19)$$

In the calculation of TDCS, we consider all 16 possible combinations of spins of participating electrons. We separately calculate TDCS with right-handed [$TDCS(\rightarrow)$] and left-handed [$TDCS(\leftarrow)$] helicity of the incident electron. The unpolarized TDCS can be calculated as:

$$(TDCS)_{unpolarized} = \frac{1}{2} [TDCS(\rightarrow) + TDCS(\leftarrow)] \quad (20)$$

We also calculate the asymmetry A in TDCS as

$$A = \frac{TDCS(\rightarrow) - TDCS(\leftarrow)}{TDCS(\rightarrow) + TDCS(\leftarrow)}. \quad (21)$$

The origin of spin asymmetry can be attributed to the spin-dependent forces, i.e., Mott scattering (due to the spin orbit interaction of the continuum electrons moving with relativistic energies in the Coulomb field of the atomic nucleus).

B. Twisted electron scattering

After having briefly recalled the basic theory used to describe the relativistic (e,2e) processes for plane-wave electron beam, we describe the same for twisted electron beam. Starting with Bessel beams we explain the twisted electron wavefunction and calculation of scattering amplitude.

1. Twisted transition amplitude

Twisted electron beams are conventionally different from plane-waves. It is superposition of plane waves (such as a Bessel beam) with a defined projection of the orbital angular momentum onto the propagation axis each with a ϕ -dependent phase. This phase leads to the characteristic twisted beam with OAM defined by the operator $\hat{L}_z = -i\hbar\partial_\phi$ with eigenvalue $\hbar l$ [31]. The simplest form of Bessel beam is provided by the solution of the Schrodinger equation in cylindrical coordinates [32]:

$$\psi_{k,l}(\mathbf{r}) = \frac{e^{il\phi}}{\sqrt{2\pi}} J_l(k_\perp, r_\perp) \frac{e^{ik_z z}}{\sqrt{2\pi}}. \quad (22)$$

This exact solution enclose the beam features which is our point of interest: the quantized (projected) OAM $\hbar l$ and the longitudinal and transverse momenta $\hbar k_z$ and $\hbar k_\perp$. In terms of its momentum components, the Bessel beam shows that this state is a ring of tilted plane waves in momentum space:

$$\psi_{k,l}(\mathbf{r}) = (-i)^l \int \frac{d\phi}{(2\pi)^2} e^{il\phi} e^{i\mathbf{k}\cdot\mathbf{r}}. \quad (23)$$

This representation has been used to calculate the elastic Coulomb scattering amplitude [32], the results of which

are useful here in simplifying some of the equations. Here we use the same formalism as used in the last section in plane wave ionization except we replace the plane wave for the incident electron with a twisted electron beam. We describe the momentum vector, \vec{k}_i , of the incident electron as;

$$\vec{k}_i = (k_i \sin\theta_p \cos\phi_p) \hat{x} + (k_i \sin\theta_p \sin\phi_p) \hat{y} + (k_i \cos\theta_p) \hat{z} \quad (24)$$

with θ_p and ϕ_p as the polar and azimuthal angles of the \vec{k}_i assuming that it propagates in the z -direction. In addition to this, the components (n_x, n_y, n_z) as discussed in Section 3.1 for incident(p) and scattered(s) electron respectively are ($\sin\theta_p \cos\phi_p, \sin\theta_p \sin\phi_p, \cos\theta_p$) and ($\sin\theta_s \cos\phi_s, \sin\theta_s \sin\phi_s, \cos\theta_s$) for the twisted electron beam.

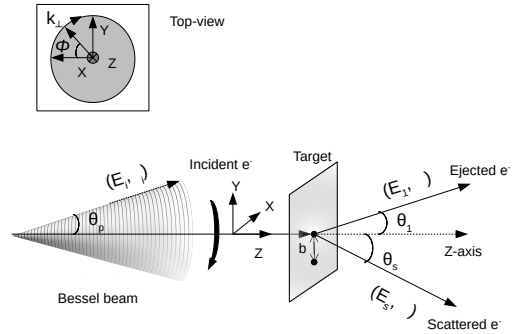


FIG. 2: Schematic diagram for the electron impact ionization of an atom by twisted electron beam in which the momentum of the beam lies on the surface of a cone with opening angle θ_p . The angular positions of the scattered and ejected electron are represented by θ_s and θ_e . The quantization (z)-axis is chosen along the propagation direction of the incoming beam. Inset shows the top view of the incident twisted electron beam. The beam is propagating into the page and twists around the propagation direction (clockwise) with phase angle ϕ . Other kinematical conditions are same as shown in the Figure 1.

Here, we assume the longitudinal momentum along the z -axis, with the polar angle being defined as the opening angle $\theta_p = \tan^{-1} \frac{k_{i\perp}}{k_{iz}}$, which can be defined as the angle the momentum vector makes with the z -axis. The perpendicular and the longitudinal components of the momentum \vec{k}_i are defined as $k_{i\perp}$ and k_{iz} .

The Bessel beam is in terms of its momentum components, which can be described as a superposition of the plane waves [32]

$$\psi_{\mathcal{Z}m}^{(tw)}(\vec{r}_i) = \int \frac{d^2 k_{i\perp}}{(2\pi)^2} a_{\mathcal{Z}m}(k_{i\perp}) e^{i\vec{k}_i \cdot \vec{r}_i}, \quad (25)$$

with the amplitude

$$a_{\mathcal{Z}m}(k_{i\perp}) = (-i)^m \sqrt{2\pi} e^{im\phi_p} \delta(|k_{i\perp}| - \mathcal{Z}), \quad (26)$$

where \varkappa is the absolute value of the transverse momentum, m is OAM number (instead of l , we use m as OAM number in this communication) and ϕ_p is the azimuthal angle (phase angle of the twisted electron beam). For the relativistic case, the wave function for the twisted electron can be described as superposition of Dirac plane wave. The wave function for the twisted electron beam can be defined as:

$$\psi_{\varkappa m}^{(tw)}(\vec{r}_i) = \int \frac{d^2 k_{i\perp}}{(2\pi)^2} a_{\varkappa m}(k_{i\perp}) u_{k,\lambda} e^{i\vec{k}_i \cdot \vec{r}_i}, \quad (27)$$

Using the equation (27) for incident twisted electron, we can write the twisted wave transition amplitude, S_{fi}^{tw} , in terms of the plane wave transition amplitude as,

$$S_{fi}^{tw}(\varkappa, \vec{q}) = \frac{(-i)^m}{2\pi} \sqrt{2\pi} \int \frac{d\phi_p}{2\pi} e^{im\phi_p - i\mathbf{k}_{i\perp} \cdot \mathbf{b}} S_{fi} \quad (28)$$

where \mathbf{b} is the impact parameter that defines the transverse orientation of the incident twisted electron beam with respect to the atom and $k_{i\perp} b = \varkappa b \cos(\phi_p - \phi_b)$ and ϕ_b is the azimuthal angle of the impact parameter \vec{b} . S_{fi} is the transition amplitude for the incident plane wave scattering for an atom, given by equation (3).

For the incident twisted electron beam, we can find the magnitude of momentum transfer to the target atom from

$$q^2 = k_i^2 + k_s^2 - 2k_i k_s \cos\theta. \quad (29)$$

where

$$\cos\theta = \cos\theta_p \cos\theta_s + \sin\theta_p \sin\theta_s \cos(\phi_p - \phi_s), \quad (30)$$

Here, θ_s and ϕ_s are the polar and azimuthal angles of the \vec{k}_s . For the coplanar geometry, $\phi_s = 0$. For the computation of the TDCS for the twisted electron, we need to compute S_{fi} from equation (3) for given ϕ_p . We use equation (28) to compute $S_{fi}^{tw}(\varkappa, \vec{q})$ by integrating over angle ϕ_p .

III. RESULTS AND DISCUSSION

We present the results of our calculations of TDCS in the Fig.3 for the charge-charge interaction $(TDCS)_0$, sum of the charge-charge and current-current interaction part $((TDCS)_{0J} = (TDCS)_0 + (TDCS)_J)$ and total contributions which includes the interference term of the matrix elements of the above contributions $((TDCS)_T = (TDCS)_0 + (TDCS)_J + (TDCS)_{INT})$. We describe $(TDCS)_0$, $(TDCS)_{0J}$, $(TDCS)_T$ by dotted, dashed and solid curves respectively and experimental data by (\bullet) . We compare our results for Cu, Ag and Au targets for the incident energy $E_i = 300\text{keV}$ (Cu and Ag) and $E_i = 500\text{keV}$ (Ag and Au) in coplanar asymmetric geometrical mode. We depict other kinematical variables of the calculation of TDCS in each frame of Fig.3. We

found that in all the calculations, our theoretical results follow the experimental trends reasonably good in the binary peak region (see peak around $\theta = \theta_q$ region, i.e. momentum transfer direction). We also note that the angular profile of $(TDCS)_0$ (dotted curve) and $(TDCS)_{0J}$ peak around $\theta = \theta_q$. However because of the interference of the scattering amplitude of the charge density and current density terms, the $(TDCS)_T$ is reduced and the binary peak is shifted to higher angle (see solid curve). In addition to this, we found that the interference term is responsible for the additional small maximum in the backward region (see solid curves in the region near to $\theta_1 = \pm 180^\circ$). From these observations, we found that our plane wave calculation reproduces the global experimental trends in the binary region and emergence of small secondary peak in the backward region. These findings are in agreement with the earlier studies of various theoretical models with the experimental data (see Physics Report of Nakel and Whelan(1999) related to relativistic (e, 2e) process). It is worth mentioning that in literature we have better theoretical models for plane wave incidence, e.g. relativistic Distorted Wave Born Approximation (rDWBA), than the one presented here for relativistic (e, 2e) processes on atoms. Therefore, the results may not be as accurate as that for the more complex theoretical model such as rDWBA. In the present scenario we compare our theoretical results to benchmark our calculations with the experimental data to ascertain that it reproduces the main trends of the angular profile of TDCS of experimental data and other theoretical models. At present, we don't have any experimental as well as theoretical results for the twisted electron beam. So the presented results should be taken as a first small step to explore this field. In future, we expect that this may lead to many more studies in the field, both at theoretical as well as experimental level, for better understanding the effect of twisted electron parameters, namely m (OAM), θ_p (opening angle) and b (impact parameter) on the relativistic (e, 2e) processes on atoms.

Now, in order to investigate the effect of the different m on the angular profile of TDCS, we present the results of $(TDCS)_0$ and $(TDCS)_T$ for $m=0.0, 0.5, 1.0, 1.5$ and 2.0 in the Fig.4. We choose same targets as used in the Fig.3 with the same kinematics used there for the plane wave (e, 2e) case. For each kinematics, we keep opening angle (θ_p) equal to the scattering angle (θ_s) with the atom located on the beam direction ($b = 0$). For example, we used $\theta_s = -9^\circ$ for Cu target at 300keV for plane wave case. We keep $\theta_p = 9^\circ$ for this case and similarly we choose θ_p for different kinematics accordingly. We present in Fig.4, the results for Cu and Ag targets at $E_i = 300\text{keV}$ for $(TDCS)_0$ in Fig.4(a) and Fig.4(c) and $(TDCS)_T$ in Fig.4(b) and Fig.4(d). We use solid, dashed, dotted, dashed-dotted, dotted-dashed-dotted curve respectively for $m= 0.0, 0.5, 1.0, 1.5$ and 2.0 . We follow the same representation throughout the paper unless otherwise stated. We plot $(TDCS)_0$ and $(TDCS)_T$ for different m in different frames to investigate the effects

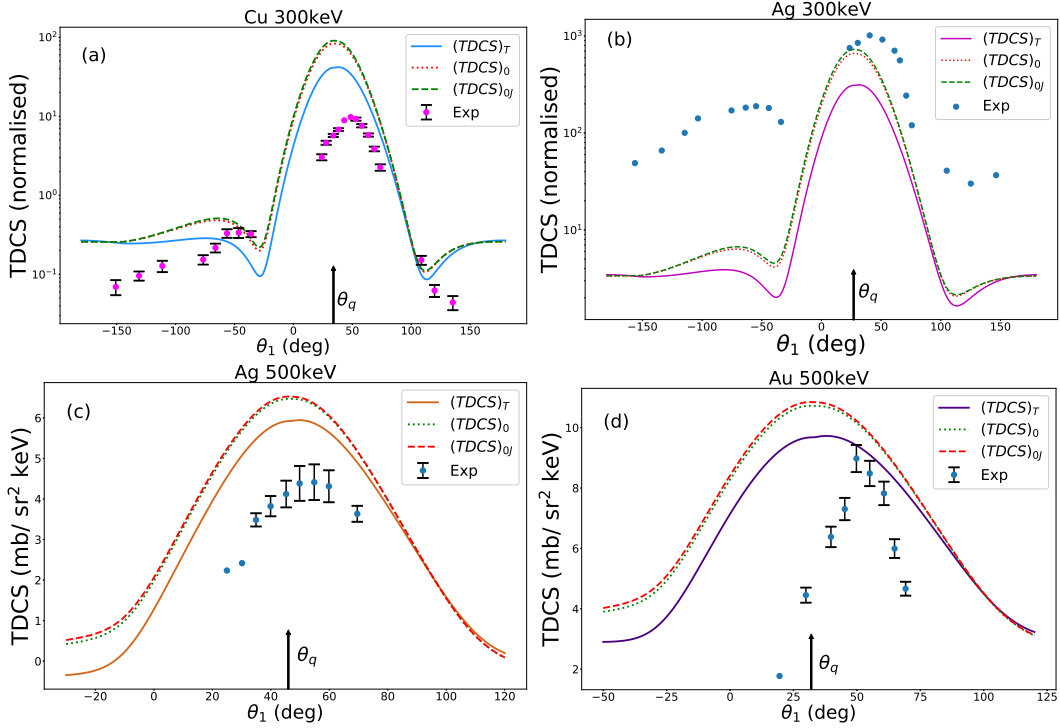


FIG. 3: $(TDCS)_T, (TDCS)_0, (TDCS)_{0J}$ are plotted as a function of the ejected electron angle (θ_1) in the coplanar asymmetry geometry mode. The experimental data points (from Nakel and Whelan [34]) are plotted as a symbol (\bullet). $(TDCS)_T, (TDCS)_0, (TDCS)_{0J}$ are represented by solid, dotted and dashed curves respectively. Kinematics for Fig(a): Cu ($E_i = 300\text{keV}, E_s = 220\text{keV}, E_1 = 71\text{keV}, \theta_s = -9^\circ$), Fig(b): Ag ($E_i = 300\text{keV}, E_s = 200\text{keV}, E_1 = 74.5\text{keV}, \theta_s = -10^\circ$), Fig(c): Ag ($E_i = 500\text{keV}, E_s = 375\text{keV}, E_1 = 100\text{keV}, \theta_s = -15^\circ$), Fig(d): Au ($E_i = 500\text{keV}, E_s = 310\text{keV}, E_1 = 100\text{keV}, \theta_s = -15^\circ$). Arrow at θ_q represents the direction of momentum transfer.

of m on charge-charge interaction ($(TDCS)_0$) and that for charge-charge and current-current interaction terms ($(TDCS)_T$). At relativistic energy regime, we expect that the current-current interaction term also dominates whereas in the non-relativistic regime, alone $(TDCS)_0$ will be sufficient to consider.

For 300keV impact energy, we observe that the binary peak of $(TDCS)_0$ shifts to lower angle for $m \neq 0$ even for our first Born approximation results. There is no significant variation in $(TDCS)_0$ for $m=0$ and $m=0.5$ case (see solid and curves of Fig 4(a) and 4(c)) other than the shifting in binary peak to lower angle and decrease of magnitude of $(TDCS)_0$ with m . However, when we observe the angular profiles of $(TDCS)_0$ for $m=1.0, 1.5$ and $m=2.0$, we found that the binary peak splits in the proximity of momentum transfer direction and a dip is formed there (see dashed, dashed-dotted and dotted-dashed-dotted curves in Fig. 4(a) and 4(c) around θ_q). The dip is more pronounced for $m=1.5$ for both Cu and Ag targets when compared to that with $m=2.0$. Having seen the angular profiles of $(TDCS)_0$, we now discuss the angular profile of $(TDCS)_T$ for $m=0.0, 0.5, 1.0, 1.5$ and 2.0 in the Fig. 4(b) and 4(d) for Cu and Ag targets respectively. When we compare $(TDCS)_T$ with the $(TDCS)_0$ for different values of m , we observe that the binary peak $(TDCS)_T$ shifts to larger angles

similar to what we observe for the plane wave calculation. Apart from this, we observe that the angular profiles of $(TDCS)_T$ follow the same patterns as found for $(TDCS)_0$, like the dominant peaks for $m = 0.0$ and $m = 0.5$ are still found for $(TDCS)_T$ (see solid and dashed curves of Fig.4(b) and Fig.4(d)). For the larger values of m the binary peak gets split and we observe two new peaks with a dip between them (see dotted, dashed-dotted and dotted-dashed-dotted curves of Fig.4 around θ_q). For Cu target, we observe that for $m = 2.0$, there is a further splitting in the angular profile (see dotted dashed-dotted curve of Fig.4(b)) resulting three peak structure in the binary region. This is not observed for Ag target (see corresponding curve in Fig.4(d)).

Having discussed results of TDCS for 300keV, we discuss the angular profile of TDCS for Ag and Au targets for given m 's for 500keV. We also increase the scattering angle and hence the opening angle ($\theta_s = -15^\circ$ and $\theta_p = 15^\circ$) to investigate the effect of momentum transfer (larger scattering angle here) and the opening angle of the Twisted beam on the angular profile of TDCS. As followed in Fig.4, we depict the various calculation of different m with the same representative curves. Here we present the $(TDCS)_0$ for plane wave calculation ($\theta_p = 0, m = 0$) to compare it with the $(TDCS)_T$ to further investigate the effect of current-

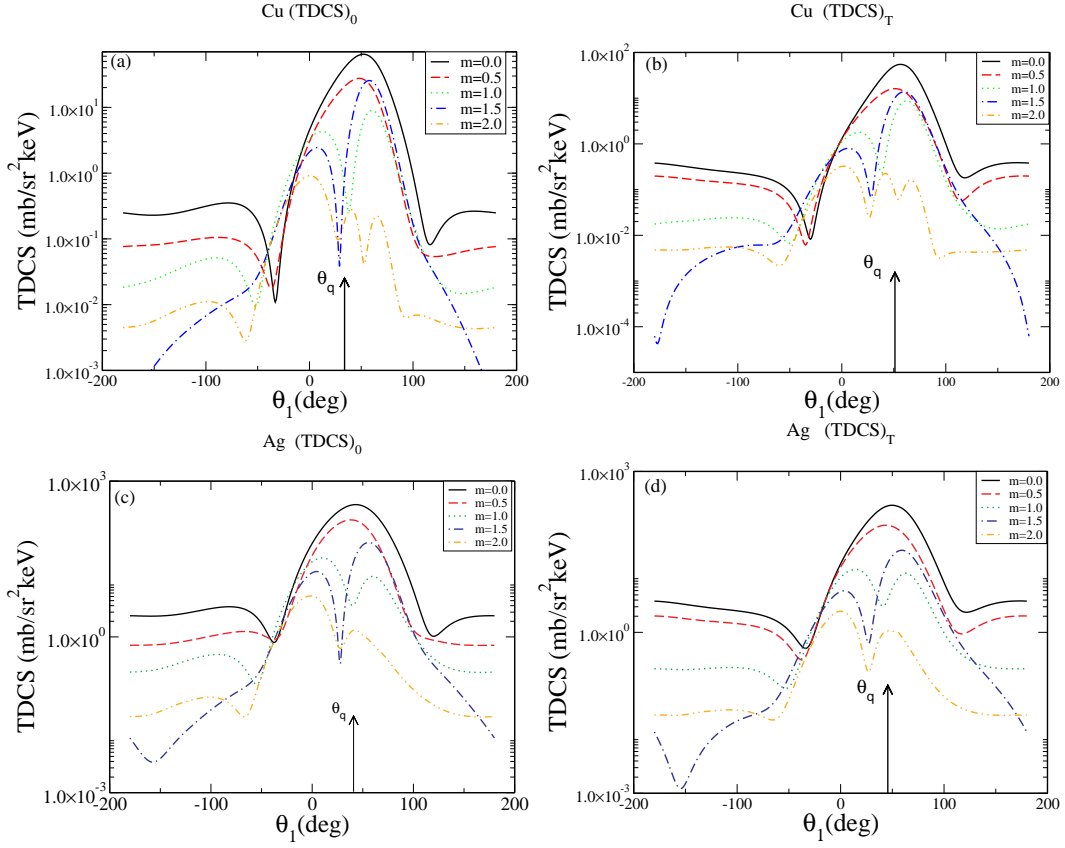


FIG. 4: $(TDCS)_0$ and $(TDCS)_T$ for $m=0.0, 0.5, 1.0, 1.5$ and 2.0 for Cu($E_i = 300\text{keV}, E_s = 220\text{keV}, E_1 = 71\text{keV}$) and Ag($E_i = 300\text{keV}, E_s = 200\text{keV}, E_1 = 74.5\text{keV}$) with $\theta_s = -9^\circ$ and $\theta_p = 9^\circ$. Fig4(a) and Fig4(c) represent $(TDCS)_0$ for Cu and Ag respectively. Similarly, Fig4(b) and Fig4(d) represent $(TDCS)_T$ for Cu and Ag.

current interaction and its interference with the charge-charge interaction. For Ag case, we found that the binary peak is not only shifted towards the momentum transfer direction, it is also enhanced (see $(TDCS)_0$ (dashed-dotted-dashed curve) and $(TDCS)_T$ (solid curve) in the Fig.5(a), $m = 0$ case). This is in complete contrast with our earlier results wherein we get binary peaks with reduced magnitude. For Au case, we get again reduced binary peak (see $m = 0$ solid curve in Fig 5(b)). When we gradually increase OAM from $m = 0.5$ to $m = 2.0$ as found in the previous calculation, the binary peak in $(TDCS)_T$ shifts to smaller angle and finally gets split for larger m , e.g. for Ag case, the splitting is found for $m = 1.0, 1.5$ and 2.0 (see dotted, dotted-dashed, dotted-dashed-dotted curves) and similarly for Au case for $m = 1.5$ and 2.0 (see dotted-dashed, dotted-dashed-dotted curves). This is worth mentioning that the splitting is not so pronounced for Au target (see Fig.5(b)) for larger m when compared that with the Ag target. In addition to this, the prominent peak in the $(TDCS)_T$ after splitting is found to be in the binary peak region for Ag target (see the split peak for $m = 1.0, 1.5$ and 2.0 in the binary region marked by arrow at θ_q in Fig.5(a)). On the other hand, we found that for Au target it is other way around. In this case, the prominent peak peaks around

15° for $m = 1.5$ and 2.0 (see Fig. 5(b)).

We discussed in Fig.4 and Fig.5 about TDCS dependence on charge-charge and current-current interactions with their interference on the scattering and opening angle of the twisted beam as well as on various values of OAM number m . We observed significant dependence of TDCS on the above mentioned kinematical parameters. In the quantum mechanical complete experiment, we need to see the effect of spin of the impinging electron on the $(e, 2e)$ process. In the case of polarized incident electron beam, the TDCS depends on the spin of the incident electron. This can be attributed to the spin orbit coupling of the electron when it is seen from the rest frame of moving electron. In the rest frame of moving electron, the intrinsic magnetic momentum of incident electron due its spin couples with the electromagnetic field of the atomic target. This leads to different types of coupling for $\lambda_+ = \frac{1}{2}$ and $\lambda_- = -\frac{1}{2}$ spin state of the incident electron beam which should be reflected in the asymmetry A of TDCS ($A = \frac{TDCS(\rightarrow) - TDCS(\leftarrow)}{TDCS(\rightarrow) + TDCS(\leftarrow)}$). In addition to this, the twisted beam carries OAM along the propagation direction so when this couples with the spin of the beam, we expect that the asymmetry should change with m . Keeping these points in mind, we plot spin asymmetry A as a function of the ejection direc-

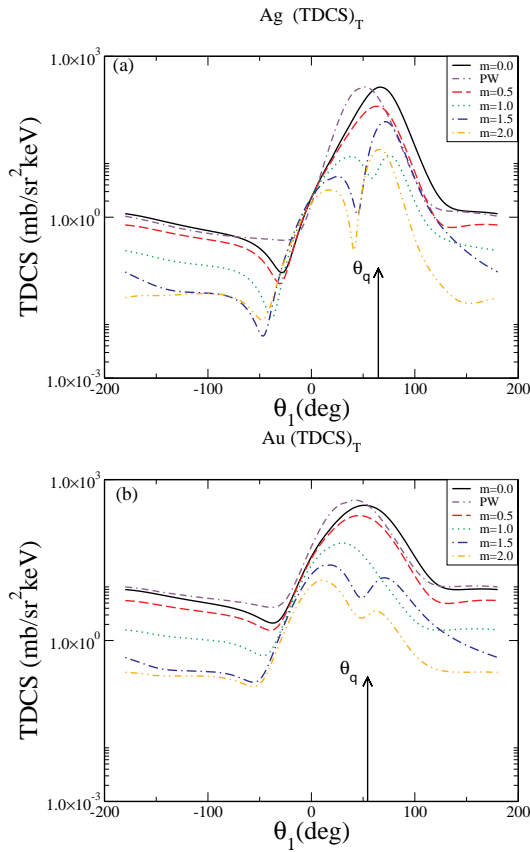


FIG. 5: $(TDCS)_T$ for Ag ($E_i = 500\text{keV}, E_s = 375\text{keV}, E_1 = 100\text{keV}$) and Au ($E_i = 500\text{keV}, E_s = 310\text{keV}, E_1 = 100\text{keV}$) targets for given m 's with $\theta_s = -15^\circ$ and $\theta_p = 15^\circ$. Here $(TDCS)_0$ for plane wave calculation ($\theta_p = 0, m = 0$) is represented by dashed-dotted-dashed line.

tion of the ejected electron for different m . We keep $E_i = 300\text{keV}$ and 500keV with different θ_s , and hence θ_p angles and choose Cu, Ag and Au targets for our calculation of A. We present the result of A in figure 6 for Cu (frame (a)), Ag at 300keV (frame (b)), Ag at 500keV (frame (c)) and Au (frame (d)) targets. The kinematics of the calculation have been shown in the figure caption. On investigating the asymmetry of A for Cu target at 300keV , we found that the asymmetry follows the same trend for $m = 0.0$ (plane wave) and $m = 0.5$ except that they follow quite different patterns in the binary peak regions (see solid and dashed curves in the region marked by arrow around $\theta = \theta_q$). For plane wave case, we found less asymmetry in the binary region where the TDCS peaks around. The same pattern is also followed for the other target's cases (see solid curve in the Fig 6(b) and 6(c) around $\theta = \theta_q$). This agrees with the similar conclusion for the elastic scattering of relativistic electrons with atom wherein the maxima in asymmetry is associated with the minima in the cross section [33] and this is also observed for the relativistic ($e, 2e$) processes on atoms with the transverse spin asymmetry [34].

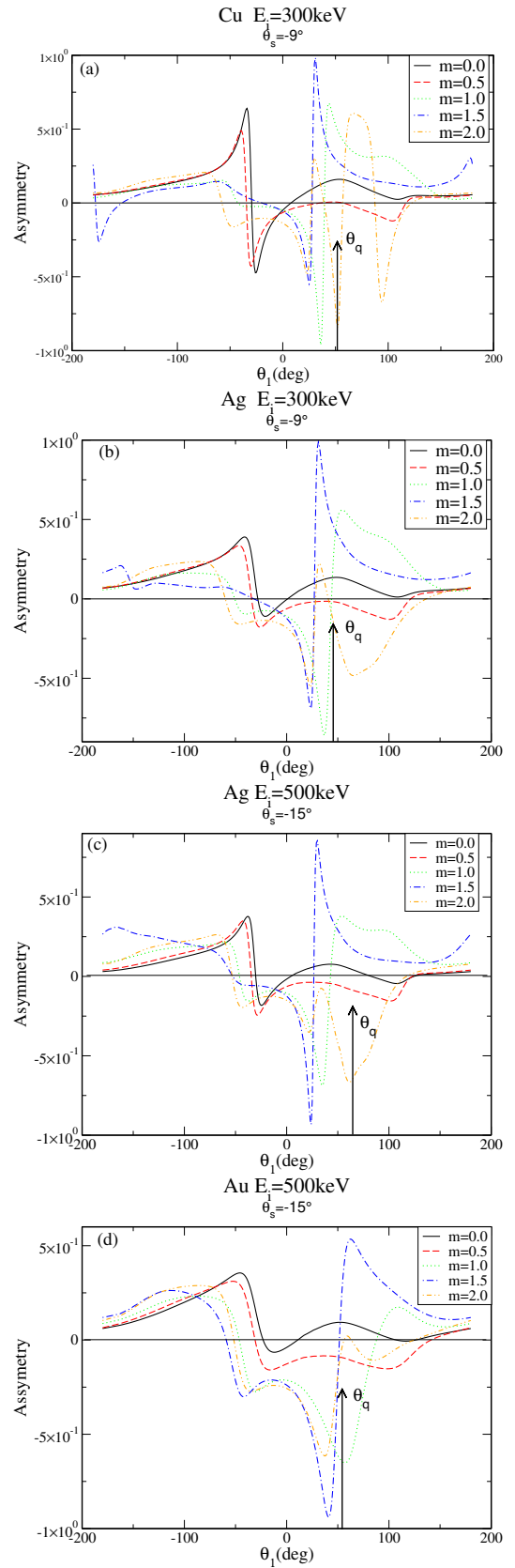


FIG. 6: Spin asymmetry A in TDCS for Cu(a), Ag($E_i = 300\text{keV}$ and $E_i = 500\text{keV}$)(b) and (c) and Au(d) respectively. Other kinematical variables are same as Fig.4 and Fig.5

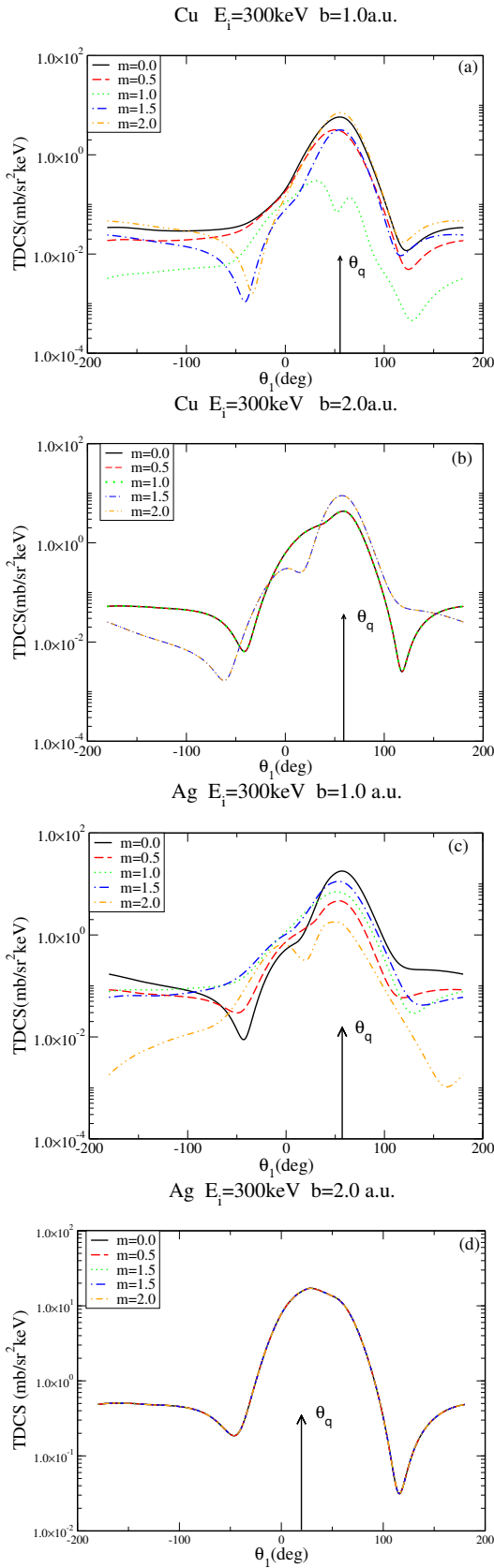


FIG. 7: $(TDCS)_T$ for Cu, Ag targets (same kinematics as Fig.4) for given m 's with impact parameter $b=1.0$ and 2.0 a.u. respectively. Fig.7.(a) and Fig.7.(b) for Cu and Fig.7.(c) and Fig.7.(d) for Ag

We found similar patterns for $m = 0.5$ for all these targets (see dashed curve of Fig.6). However, we get different patterns for $m = 1.0, 1.5,$ and 2.0 , especially in the binary peak region. We get substantial asymmetry A in the binary region and also oscillatory (see dotted, dashed-dotted and dotted-dashed-dotted curves of Fig.6 in the region $\theta_1 = \theta_q$). Especially, for Cu target, we see drastic change in the asymmetry for all the values of m (see dotted, dashed-dotted and dotted-dashed-dotted curves in Fig.6(a)). Further, when we compare the similar calculation of A for Ag target with that for Cu target, we found that except for $m = 2.0$, the asymmetry for Ag target is not as oscillatory as that for Cu target (compare the dotted-dashed-dotted curves of figure 6(a) and 6(b)). When we compare it with Au target we found that the asymmetry for the different m don't change abruptly and follow gentle behaviour with the angle θ_1 . The asymmetries here are less oscillatory (see Fig.6(d)) as compared to the other two cases (see Fig.6(a),6(b) and 6(c) for comparison with the Fig.6(d)). Finally, we observe that the asymmetry in Cu and Ag oscillates between $+1$ to -1 and 0.8 to -1.0 respectively. However, it oscillates between 0.5 to -0.9 for Au target. Here we remark that both the angular profiles of TDCS and spin asymmetry depends on the OAM number m of the twisted electron beam and also on the atomic number Z .

Finally, we investigate the angular profile of TDCS of the twisted electron beam for the impact parameter $b=1.0$ and 2.0 a.u. for the three targets. We follow the same convention for different m values as discussed previously. For all the three targets, we see $(TDCS)_T$ profiles follow a reduction in number of peaks as we change b value along with m values. For Cu target at 300keV for $b=0.0\text{a.u.}$ (see Fig.4(b)), we see there is a two peak structure and a three peak structure for $m=1.0$ and $m=2.0$ respectively. In case of $b=1.0\text{a.u.}$ (see Fig.7(a)), there is a similar two peak structure for $m=1.0$ but for $m=2.0$ there is no three peak structure as such. As we further change b to 2.0a.u. , peaks which arise in case of $b=0.0\text{a.u.}$ vanish for $m=1.0$ and 2.0 . Overall for Cu as we change b from 0.0 to 2.0a.u. the curves become smooth with no pronounced dips which were observed for $b=0.0\text{a.u.}$ case. For Ag target, we plot the TDCS profiles for impact energies 300keV (see Fig.7(c) and Fig.7(d)) and 500keV (see Fig.8(a) and Fig.8(b)) for $b=1.0\text{a.u.}$ and $b=2.0\text{a.u.}$ respectively. We observe that for $b=1.0\text{a.u.}$ (Fig.7(c)), $(TDCS)_T$ profile shows a two peak structure for $m=2.0$ and for $b=2.0\text{a.u.}$ all the $(TDCS)_T$ profiles are merged yielding a single profile. For the same target Ag with higher energy for $b=1.0\text{a.u.}$ (Fig.8(a)) the peak in the binary region is shifted more towards 0° as we increase m . Finally for $m=1.5$ and 2.0 a two peak structure arises. For $b=0.0\text{a.u.}$ (see Fig.4(d)), case the binary peaks are prominent with a dip around 50° when compared to $b=1.0\text{a.u.}$ and $b=2.0\text{a.u.}$ cases for all m values for Ag target. Similarly comparing for Au target at 500keV impact energy with different b when we increase b from $b=0.0\text{a.u.}$ (see Fig.5(b)) to $b=1.0\text{a.u.}$ (see Fig.8(c))

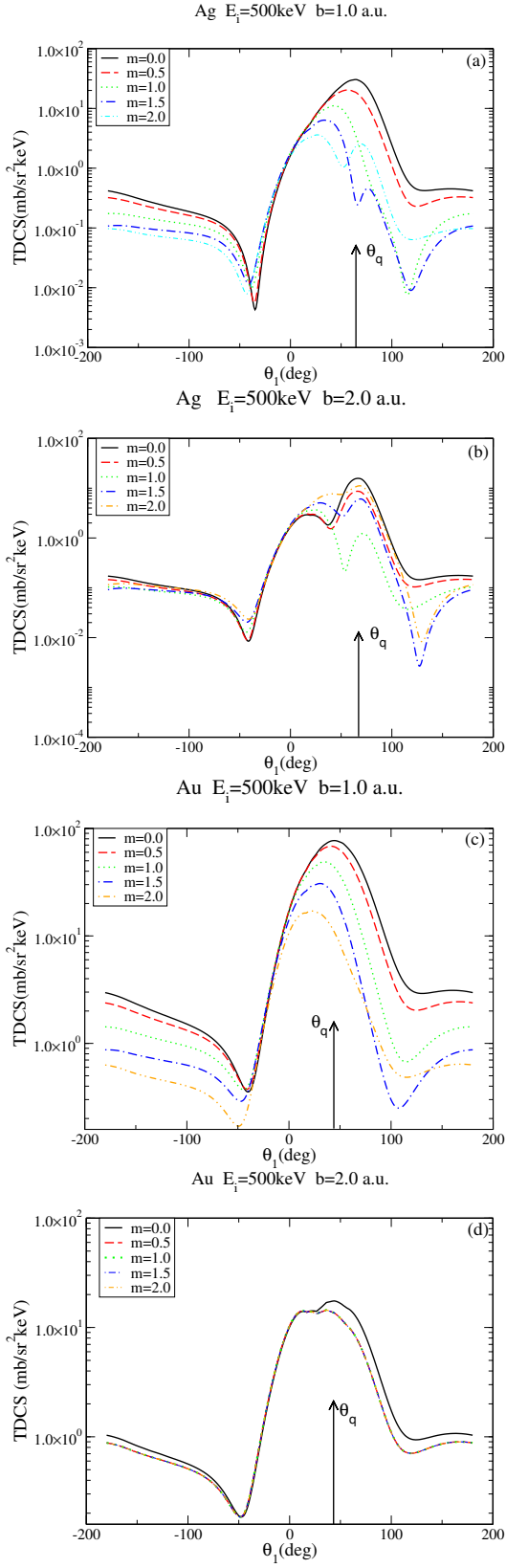


FIG. 8: $(TDCS)_T$ for Ag and Au targets (same kinematics as in Fig.5) for given m 's with impact parameter $b=1.0$ and 2.0 a.u.. Fig8.(a) and Fig8.(b) for Ag target and Fig8.(c) and Fig8.(d) for Au target.

the peak in the binary region is gradually shifted from 45° to 25° while we change m value and finally when we change b to 2.0 a.u.(Fig.8(d)) we observe that the TDCS angular profile gets confined to one broad peak which is little bit flat with a hump in the binary peak region.

IV. CONCLUSION

In this paper, we have studied the relativistic electron impact ionization of heavy atomic targets namely Cu, Au and Ag by twisted electron beam in coplanar asymmetric geometrical mode in the first Born approximation. A range of kinematical parameters were used in order to study the effect of various parameters of the twisted electron beam on $(e,2e)$ process, namely opening angle (θ_p), OAM number (m) and impact parameter (b). The spin asymmetry in TDCS caused by polarized incident electron beam is presented to interpret the effects of twisted electron beam on relativistic $(e,2e)$ process. We studied TDCS for the charge density, sum of the charge and current density's part and total contributions which includes the interference term of the matrix elements of the said terms. We observed that TDCS depends significantly on charge-charge and current-current interactions with their interference on the opening angle (θ_p) and OAM number m of the twisted beam. As per the results both the angular profiles of TDCS and spin asymmetry depends on the OAM number m of the twisted electron beam and also on the atomic number Z . Added to this the profiles of asymmetry in case of Cu is particularly interesting with higher value of OAM number and we are exploring it further. And we are working towards betterment of our proposed theoretical model.

This is worth mentioning that, to the best of our knowledge, this is the first attempt in literature to describe relativistic electron impact ionization of heavy atomic targets by twisted electron beam in coplanar asymmetric geometry. In our theoretical model we have neglected exchange-correlation effect arising from the many-electron aspect for heavy atomic targets. Although there are better models as compared to our model like rD-WBA (relativistic Distorted Wave Born Approximation) for plane wave incidence which can be explored for various heavy atomic targets for the twisted electron case. Effect of different kinds of relativistic wave-function can be considered instead of semi-relativistic Coulomb wave-function to elucidate some more effects of twisted electron beam on relativistic $(e,2e)$ process as explained earlier. Further, one can study the effects of higher values of OAM number m of Twisted electron beam with varied impact energy on the $(e,2e)$ process. Also it would be interesting to investigate asymmetry for these targets with higher OAM number m . Different kinematics, such as coplanar symmetric geometry, non-coplanar geometries, Bethe-Ridge kinematics etc. can be considered. Experimentally more work is expected for multi-electronic targets to explore this area deeply. Although at present we

don't have as such extensive experimental data as well as theoretical results for the twisted electron beam except relativistic (e,2e) case with plane wave, still we expect this may lead to many more studies in the field of electron impact ionization and twisted electron beam, both at theoretical level as well as experimental level for a fundamental understanding of interaction of twisted electron (Bessel) beam with multi-electron atomic targets.

Acknowledgement

Authors acknowledge the Science and Engineering Research Board, Department of Science and Technology, Government of India, for funding the project through the Grant number EMR/2016/003125.

-
- [1] Ian E. McCarthy and Erich Weigold, Cambridge monographs on atomic, molecular and Chemical Physics.
- [2] V. G. Neudatchin and F. A. Zhivopistsev, Phys. Rev. Lett. 32, 995 (1974)
- [3] Yu. F. Smirnov and V. G. Neudatchin, Zh. Eksp. Teor. Fiz., Pisma 3, 298 (1966) [JETP Lett.3, 192 (1966)]
- [4] M. Vos and I. E. McCarthy, Rev. Mod. Phys. 67, 713 (1995)
- [5] V. G. Neudatchin, Yu V. Popov and Yu. F. Smirnov, Phys. Uspekhi 42, 1017-1044 (1999)
- [6] B. H. Bransden and C. J. Joachain Physics of Atoms and Molecules (Second edition) 1988.
- [7] H. Ehrhardt, M. Schultz, T. Tekaas, K. Willmann, Phys. Rev. Lett. 22 (1969) 89.
- [8] U. Amaldi, A. Egidi, R. Marconero, G. Pizzella, Rev. Sci. Instr. 40 (1969) 1001-1004.
- [9] C.T. Whelan, H.R.J. Walters, A. Lahmam-Bennani, H. Ehrhardt, (e,2e) & Related Processes, Kluwer, Dordrecht, 1993.
- [10] C.T. Whelan, H.R.J. Walters, Coincidence Studies of Electron and Impact Ionization, Plenum, New York, 1997.
- [11] A. Lahmam-Bennani, J. Phys. B 24 (1991) 2401.
- [12] Salim Houamer, Mehdi Chinoune and Claude Dal Cappello, Eur. Phys. J. D (2017) 71: 17
- [13] E. Schule, W. Nakel, J. Phys. B 15 (1982) L639-L641.
- [14] H-Th. Prinz, K-H. Besch, W. Nakel, Phys. Rev. Lett. 74 (1995) 243.
- [15] K. Y. Bliokh, Y. P. Bliokh, S. Savel'ev, and F. Nori, Phys. Rev. Lett. 99, 190404 (2007).
- [16] M. Uchida and A. Tonomura, Nature (London) 464, 737 (2010).
- [17] J. Verbeeck, H. Tian, and P. Schattschneider, Nature (London) 467, 301 (2010).
- [18] B. J. McMorran, A. Agrawal, I. M. Anderson, A. A. Herzog, H. J. Lezec, J. J. McClelland, and J. Unguris, Science 331, 192 (2011).
- [19] J. Rusz and S. Bhowmick, Phys. Rev. Lett. 111, 105504 (2013).
- [20] A. Beche, R. Van Boxem, G. Van Tendeloo, and J. Verbeeck, Nat. Phys. 10, 26 (2013).
- [21] P. Schattschneider, S. Löffler, M. Stoger-Pollach, and J. Verbeeck, Ultramicroscopy 136, 81 (2014).
- [22] V. Serbo, I. P. Ivanov, S. Fritzsche, D. Seipt, and A. Surzhykov, Phys. Rev. A 92, 012705 (2015).
- [23] D. V. Karlovets, G. L. Kotkin, and V. G. Serbo, Phys. Rev. A 92, 052703 (2015).
- [24] I. P. Ivanov, V. G. Serbo and V. A. Zaytsev, Phys. Rev. A 93, 053825 (2016).
- [25] D. V. Karlovets, G. L. Kotkin, V. G. Serbo and A. Surzhykov, Phys. Rev. A 95, 032703 (2017).
- [26] A. V. Maiorova, S. Fritzsche, R. A. Müller and A. Surzhykov, Phys. Rev. A 98, 042701 (2018).
- [27] Bliokh K, Ivanov I, Guzzinati G, et al. Theory and applications of free-electron vortex states. Phys Rep.2017; 690:1-70.
- [28] A L Harris , A Plumadore and Z Smozhanyk J. Phys. B: At. Mol. Opt. Phys. 52, 094001 (2019)
- [29] R. Choubisa and Munendra Jain Phys. Rev. A 86, 022702 (2012)
- [30] A. S. Bhullar and K. K. Sud, Indian J. Phys. B 73, 299 (1999).
- [31] R. Van Boxem, B. Partoens, and J. Verbeeck, Rutherford scattering of electron vortices, Phys. Rev. A 89, 032715 (2014).
- [32] R. Van Boxem, B. Partoens, and J. Verbeeck, Phys. Rev. A 91, 032703 (2015).
- [33] R. Choubisa J. Phys. B: At. Mol. Opt. Phys. 48, 045201 (2015)
- [34] W. Nakel, C.T. Whelan Physics Reports 315 (1999) 409-471